CHINESE OPTICS LETTERS

Vol. 21, No. 12 | December 2023

Experimental demonstration of TE/TM polarization-independent frequency upconversion assisted by polarization coupling

Tingting Ding (丁婷婷)[1], Yongzhi Tang (唐永志)[2], Xuerui Sun (孙雪芮)[2], Yiwen Huang (黄义文)[2], Bei Jiang (江 蓓)[1], Jin Liu (刘 瑾)[1], Zhiwei Li (李志伟)[1], Yuanlin Zheng (郑远林)[2,3*], and Xianfeng Chen (陈险峰)[2,3,4**]

[1] School of Electronic and Electrical Engineering, Shanghai University of Engineering Science, Shanghai 201620, China

[2] State Key Laboratory of Advanced Optical Communication Systems and Networks, School of Physics and Astronomy, Shanghai Jiao Tong University, Shanghai 200240, China

[3] Shanghai Research Center for Quantum Sciences, Shanghai 201315, China

[4] Collaborative Innovation Center of Light Manipulation and Applications, Shandong Normal University, Jinan 250358, China

*Corresponding author: ylzheng@sjtu.edu.cn

**Corresponding author: xfchen@sjtu.edu.cn

Received March 10, 2023 | Accepted July 14, 2023 | Posted Online November 20, 2023

Optical frequency conversion based on the second-order nonlinearity ($\chi^{(2)}$) only occurs in anisotropic media (or at interfaces) and thus is intrinsically polarization-dependent. But for practical applications, polarization-insensitive or independent operation is highly sought after. Here, by leveraging polarization coupling and second-order nonlinearity, we experimentally demonstrate a paradigm of TE/TM polarization-independent frequency upconversion, i.e., sum frequency generation, in the periodically poled lithium niobate-on-insulator ridge waveguide. The cascading of quasi-phase-matched polarization coupling and nonlinear frequency conversion is exploited. With a proper transverse electric field, TE and TM mode fundamental waves can be frequency-upconverted with an equal efficiency in the frequency converter. The proposed method may find ready application in all-optical wavelength conversion and upconversion detection technologies.

Keywords: frequency upconversion; polarization coupling; lithium niobate on insulator; ridge waveguide; cascading process.

DOI: 10.3788/COL202321.121901

1. Introduction

Lithium niobate (LN) is a multifunctional ferroelectric crystal with the exceptional properties of having a wide transparent window, a large nonlinear and electro-optic (EO) coefficient, etc. It is widely used in applications such as nonlinear optics and optical telecommunication. The strong second-order nonlinearity ($\chi^{(2)}$) of LN lies in the pivot of many applications such as laser wavelength extension[1,2], nonlinear optical manipulation[3,4], all-optical conversion and processing[5–7], and upconversion generation/detection protocols[8–10], where frequency conversion like second-harmonic generation (SHG) and sum-/difference frequency generation (SFG/DFG) plays a vital role. In principle, spatial symmetry rules out second-order nonlinearity in bulk isotropic media, making $\chi^{(2)}$ nonlinearity-based frequency conversion intrinsically polarization-dependent or sensitive. In addition, the tensor elements of the nonlinear susceptibility vary for different polarization light (e.g., $d_{33} = 27$ pm/V, $d_{31} = 4.5$ pm/V for LN), leading to highly unequal conversion efficiency (positively proportional to d_{eff}^2, where d_{eff} is the effective nonlinear coefficient). At present, nearly all $\chi^{(2)}$ nonlinear devices operate in the polarization-sensitive mode, which restricts their applications. There has been intense desire to obtain polarization-independent operation for frequency conversions, because the polarization state of light is not maintained in fibers or in space in many real applications, such as optical communication and quantum systems.

Many efforts have been devoted to addressing this issue. A straightforward solution is to divide the quasi-phase-matched (QPM) crystal [e.g., periodically poled lithium niobate (PPLN)] into two sections for two-stage frequency conversion, where SHG of each polarization component takes place in different sections. Dual-period QPM structures are also feasible. By careful waveguide dispersion engineering, it is possible to reach simultaneous QPM conditions for both TE and TM modes with

© 2023 Chinese Optics Letters

one single poling period but at a specific wavelength[11]. In quantum optics, type-I spontaneous parametric downconversion (SPDC) photon entanglement sources typically utilize a two-crystal geometry, which employs two adjacent, orthogonally aligned thin nonlinear crystals (e.g., BBO) for phase matching[12]. The scheme has also been adopted in the frequency conversion of vector beams[13,14]. The orthogonal polarization component of the fundamental wave is frequency-converted in each quadratic crystal. However, the conversion efficiency is limited, as a short interaction length is required. Polarization-insensitive frequency upconversion has also been demonstrated by using a polarization Sagnac nonlinear interferometer based on type-0 phase matching for dual-polarization-mode frequency conversion[15]. A polarization diversity configuration is also an alternative solution[16,17]. Horizontally and vertically polarized components of the input are separated and fed to two frequency converters. The system is complex and difficult in balancing the dual channels. Still, realizing polarization-independent frequency conversion remains a challenge. A simple solution to address this issue would be of significance for practical applications.

Additionally, the EO effect, arising from the nonspatial symmetry of materials, is also intrinsically polarization-dependent. To access a specific EO coefficient element, an electric field should be applied along a certain direction. The strong EO effect of LN has been exploited for high-speed optical modulators for decades, and the recent lithium niobate on insulator (LNOI) technology has propelled the performance and applications of EO modulators to new heights[18–20]. Transverse EO effect is an ideal way to achieve phase modulation, which is mostly adopted in phase, intensity, and polarization modulators[21–26]. Polarization modulators can either exploit polarization conversion under transverse EO effect[24,25], or phase modulation with polarization multiplexing[26].

Here, we propose a paradigm to address the polarization dependence issue in $\chi^{(2)}$ nonlinear wave mixing. By leveraging the transverse EO effect and second-order nonlinearity, we demonstrate cascaded polarization coupling and sum-frequency generation (SFG) in a periodically poled lithium niobate-on-insulator (PPLNOI) ridge waveguide. TE/TM polarization-independent frequency upconversion is experimentally obtained in a single PPLNOI ridge waveguide via the cascading process. Results show that with a proper transverse electric field, the SFG conversion efficiency for both TE and TM mode inputs is the same in the PPLNOI waveguide. Taking the advantages of the LNOI ridge waveguide, the applied voltage is as low as 14.1 V in our device. The conversion efficiencies for TE- and TM-polarized inputs are balanced from 0:1 to 0.3:0.3, making the frequency upconversion independent with respect to TE/TM-polarized input.

2. Theory Simulation and Experiment Conditions

To obtain TE/TM polarization-independent operation, we introduce both polarization coupling and frequency conversion (e.g., SFG) in a single PPLNOI waveguide. The wave mixing consists of quasi-phase-matched (QPM) *e–o* polarization coupling ($\omega_{1z} \leftrightarrow \omega_{1y}$) and *ee–e* (type-0) SFG ($\omega_{1z} + \omega_{2z} \rightarrow \omega_{3z}$). The QPM condition for both processes, or the cascading condition, can be met in the PPLNOI waveguide with one QPM period, when $\Delta k_{\mathrm{PC}} = \Delta k_{\mathrm{SFG}} = G$, where Δk is the phase mismatch and the subscript refers to the wave-mixing process. $G = 2\,m\pi/\Lambda$ is the reciprocal vector of the PPLNOI waveguide, with m being the QPM order and Λ being the poling period.

Figure 1(a) schematically shows the concept of the TE/TM polarization-independent operation of SFG in our device based on the PPLNOI ridge waveguide. The input FW_1 undergoes polarization coupling in the waveguide affected by a TE field. Thus, both TE and TM polarization components are present in the waveguide. The TM-polarized FW_1 is then frequency upconverted at the presence of the TM-polarized pump, FW_2, to generate the sum frequency, SF. The polarization configuration can utilize the largest nonlinear coefficient, d_{33}, of LN. In our experiment, the PPLNOI ridge waveguide was fabricated from a 5.0-μm thick PPLNOI chip (z-cut) via the optical grade dicing method. The depth of the dicing grooves is approximately 2.5 μm. The waveguide has a cross-sectional dimension of 6.0 μm (width) × 5.0 μm (height), and has a length of 10 mm. The period of the QPM grating is 20.5 μm with a duty cycle of 50%, designed for QPM polarization coupling at the telecom band. A pair of metallic (Ni/Cr) electrodes is placed on both sides of the waveguide for voltage applying. The loss induced by metallic absorption is small for the microscale ridge waveguide, whose main part comes from coupling loss and waveguide scattering. The proof-of-principle implementation is carried out using the experimental setup shown in Fig. 1(b). Two tunable lasers (1500 to 1600 nm) are used as the fundamental wave (FW) sources (FW_1 and FW_2), whose polarization is separately

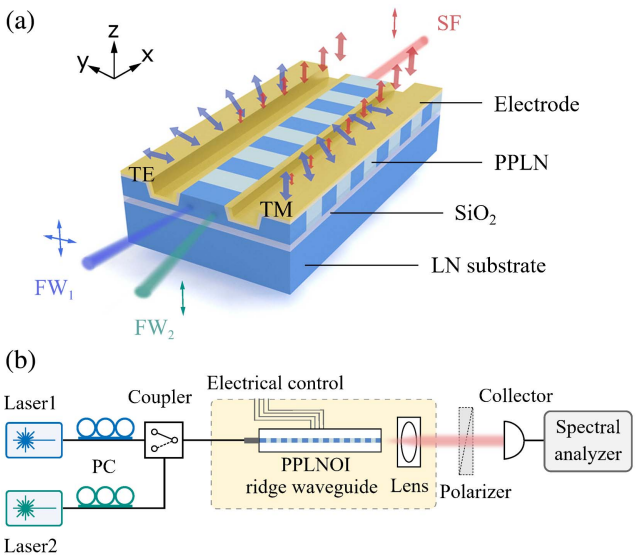

Fig. 1. (a) Schematic of the cascading of polarization coupling and SFG, showing TE/TM-independent operation during the frequency upconversion; (b) experimental setup.

controlled by a polarization controller (PC). They are combined by a 50:50 coupler and fed into the PPLNOI ridge waveguide. The power of each wave fed into the waveguide is approximately 10 mW. The device is temperature-controlled at an accuracy of 0.1°C. The setup is similar to our previous demonstration of cascaded PC and SHG/SFG[27,28], where TE/TM polarization-independent operation was not investigated.

To analyze the cascading process, we adopt the coupled-mode theory and a simplified model of plane wave approximation. Assuming QPM cascading condition ($\Delta k = 0$) is met, we can get the wave-mixing equations from the coupled-mode theory, which read as follows:

$$\frac{dA_{1z}}{dx} = -\frac{i\omega_1}{2n_{1z}c}(\kappa A_{1y} + 2d_{\text{eff}}A_{2z}^{*}A_{3z}) - \alpha A_{1z}, \tag{1}$$

$$\frac{dA_{1y}}{dx} = -\frac{i\omega_1}{2n_{1y}c}\kappa A_{1z} - \alpha' A_{1y}, \tag{2}$$

$$\frac{dA_{2z}}{dx} = -\frac{i\omega_2}{n_{2z}c}d_{\text{eff}}A_{1z}^{*}A_{3z}, \tag{3}$$

$$\frac{dA_{3z}}{dx} = -\frac{i\omega_3}{n_{3z}c}d_{\text{eff}}A_{1z}A_{2z}. \tag{4}$$

Here, A is the amplitude of each wave, ω is the angular frequency, and n is the refractive index. Subscripts 1, 2, and 3 represent FW_1, FW_2, and SF, respectively. FW_2 is the pump wave and is considered undepleted in the small signal approximation. κ is the electro-optical coupling coefficient and $\kappa = -\gamma_{51}E_y n_{1y}^2 n_{1z}^2 g$, where γ_{51} is the electro-optic coefficient, E_y is the applied TE field, and g is the Fourier amplitude of the reciprocal vector G. d_{eff} is the effective nonlinear coefficient. α and α' are the propagation loss for TM- and TE-polarized fundamental waves, respectively. They are typically different in realistic applications. c is the speed of light. The coupled equations are then numerically calculated in an interaction length of 1 cm. The simulation results are plotted in Fig. 2, which is nearly the same at different wavelengths at the telecommunication bands.

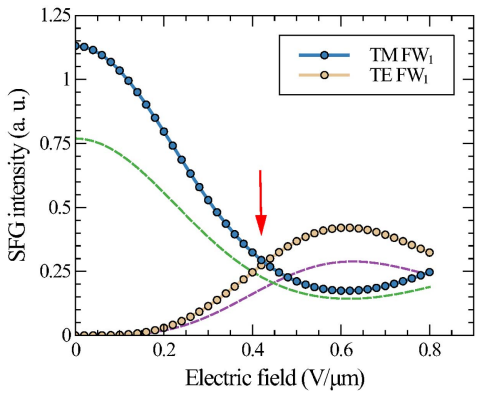

Fig. 2. Simulation of the SF output with respective to TE/TM-polarized FW_1 input.

The crossing point of the curves implies a condition where the SF output or conversion efficiency is balanced for both TE- and TM-polarized FW_1 inputs. At this point, the polarization coupling assisted upconversion becomes TE/TM polarization-independent. The corresponding electric field is about 0.43 V/μm for the ideal case.

We also investigate the coupling dynamics considering different propagation loss, α and α', which is inevitable in applications. The loss difference may originate from polarization-dependent absorption/scattering, fiber–waveguide coupling, and other factors. The coupling dynamics is still similar if the loss for TE and TM modes is different. A typical result ($\alpha = 2\alpha' = 0.2\,\text{cm}^{-1}$) is as the dashed line indicated in Fig. 2. More importantly, the crossing or the balance still exists. This means that there is always a specific intensity of electric field to obtain the TE/TM-independent operation, and the working point is robust. The feature can be utilized and would also be appealing in realistic applications.

3. Results and Discussion

First, polarization coupling is carried out using one laser source. A polarizer and an NIR detector are placed after the collimated output. Polarization coupling occurs at the wavelength of FW_1. The tuning result is plotted in Fig. 3(a). The tuning slope of polarization coupling of FW_1 is measured to be −0.85 nm/°C. Then, the cascading experiment is carried out using both laser sources. The harmonic output of FW_1 and FW_2 is collected and monitored using a spectral analyzer. With micrometer-scale dimensions, harmonic waves at higher spatial mode orders can be excited in the multimode waveguide during nonlinear wave

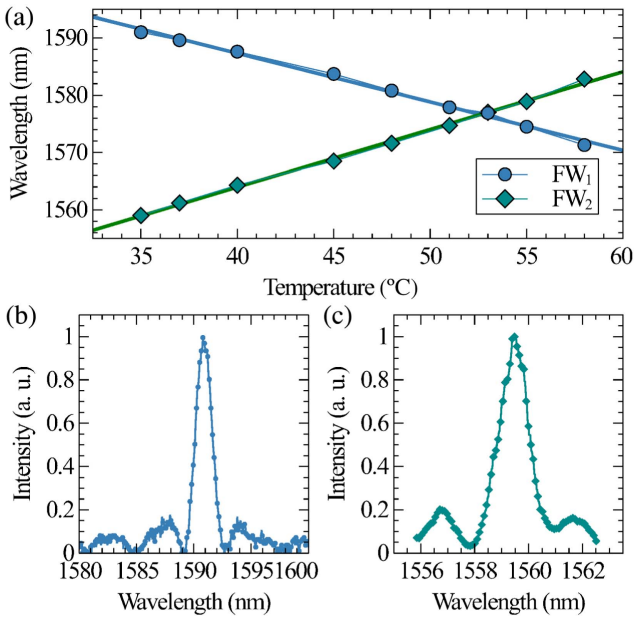

Fig. 3. (a) Temperature tuning of polarization coupling for FW_1 and the corresponding FW_2 in SFG; (b) phase-matching tuning curve of polarization coupling; (c) phase-matching tuning curve of SFG.

mixing. During the experiment, QPM SFG is observed between the FW at the fundamental spatial mode and SF at a higher spatial mode. The tuning result is also plotted in Fig. 3(a). The tuning slope of SFG is measured to be 1.0 nm/°C. As the temperature varies, the simultaneous polarization coupling and SFG can be achieved by tuning the wavelengths of FW_1 and FW_2 accordingly. The cascading condition can be accessed in a relatively wide wavelength range. This feature is favored for practical applications.

At the temperature of 35°C, the cascading condition requires the wavelengths of FW1 and FW_2 to be 1591.0 and 1559.5 nm, respectively. The spectra for polarization coupling and SFG are shown in Figs. 3(b) and 3(c). Both have a line shape of the sinc function. The full width at half-maximum (FWHM) of the polarization coupling QPM spectrum is 1.6 nm, and the FWHM of the SFG QPM spectrum, as we scan the wavelength of FW_1 while keeping that of FW_2 fixed, is 1.3 nm. The wavelength tolerance of the cascading has an FWHM of about 1 nm. The spectrum of the harmonic output is shown in Fig. 4(a). When FW_1 wave is TE mode (FW_2 wave is kept to be TM mode), only its SHG at 779.75 nm without SFG signal can be observed. The *oe–e* type SFG is not phase-matched. When both FW_1 and FW_2 waves are TM-polarized, both SHG and SFG take place in the waveguide. The left and right sideband peaks correspond to the SHG signals of FW_1 and FW_2 at 779.75 and 795.50 nm, respectively. The middle high peak at 787.55 nm is the SFG signal of the two. The device is highly polarization-sensitive, as determined by the nature of the second-order nonlinearity. The intensity of the generated SF signal is linearly dependent on the power of FW_2, consistent with the theory prediction, as shown in Fig. 4(b). At present, the conversion efficiency of approximately 10^{-4} $W^{-1}\cdot cm^{-2}$, the same as in previous reports[27,28], is relatively low, as compared with the state-of-the-art results. This is because SFG is only QPM between different spatial mode orders with a small overlapping factor. Higher conversion efficiency can be expected with a more proper QPM period to guarantee phase matching between the fundamental spatial order of the two modes in the waveguide with a smaller cross section. The experimental normalized conversion efficiency for perfect QPM SHG in similar ridge waveguides has been reported to be 62% $W^{-1}\cdot cm^{-2}$[29].

For TE- and TM-polarized FW_1 inputs (FW_2 is always kept to be TM-polarized), the SFG signal can be electrically controlled via the cascading process. The output with respect to the applied voltage is shown in Fig. 5. The cascading process hints at a working point where the output can be insensitive to the input polarization, i.e., a TE/TM polarization-independent operation. The intersection point of the two curves clearly shows the existence of such a condition. In our experiment, when the applied voltage is 14.1 V, the SFG output value is the same for both TE and TM inputs, as marked by the arrow. This is the critical condition when the device becomes TE/TM polarization-independent. The efficiency is 30% of that for the TM-polarized input. The actual voltage is multiple times larger than the theoretical prediction, which may result from the inefficiency of the electrodes. The effective gap of the electrodes is much larger than the waveguide width. Although the conversion efficiency is reduced, it can be compensated for by increased pump power for SFG. It is worth noticing that this characteristic can be observed at different wavelengths; see also Fig. 3(a). But the wavelength of FW_2 has to be kept away from the polarization coupling condition to avoid decreased effective pump power when the voltage is applied. The suitable working temperature of this device is from room temperature to 47°C. As shown in Fig. 5, the polarization dependence as represented by the conversion efficiency ratio between TE- and TM-polarized inputs is balanced from 0:1 (0 for phase mismatched conversion and 1 for normalized perfect QPM) to 0.3:0.3. It is worth mentioning that the transmission or loss inequality between the TE and TM modes in the device has been included. Loss or coupling difference between TE and TM modes in the waveguide can be directly compensated, while the issue needs careful balancing in polarization diversity configuration. The difference can be easily cancelled out by tuning the applied voltage in our scheme. Thus, a TE/TM polarization-independent frequency conversion scheme is established.

As previously mentioned, to address the polarization sensitiveness of frequency conversion based on the second-order nonlinearity, the polarization multiplexing scheme introduces additional complexities and redundancies to the device. And the method requires precision balancing of the optical loss

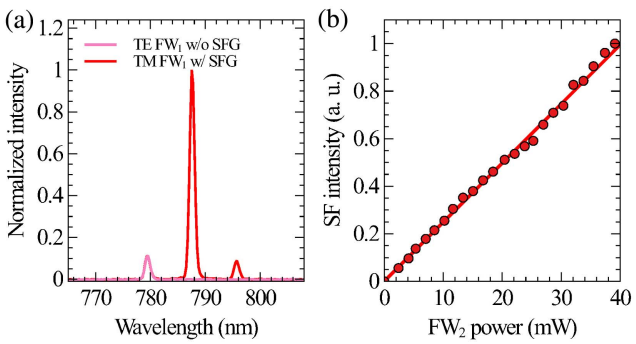

Fig. 4. (a) Spectrum of the SFG signal, as well as SHG of each wave, with TE or TM FW_1 input; (b) SFG intensity as a function of the pump power of FW_2.

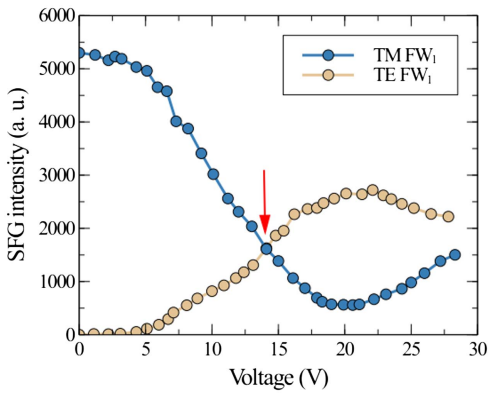

Fig. 5. Upconverted SFG signal as a function of the applied voltage for TE/TM FW_1 input. FW_2 is the TM mode and unaffected by the applied electric field.

and conversion efficiency for both polarizations in advance. In our scheme, by a simple modification to the PPLNOI ridge waveguide, the frequency converter can work in a TE/TM polarization-independent mode, and the balancing can be achieved by tuning the applied voltage. It can be envisioned that such a scheme may be of use in applications such as all-optical wavelength conversion and upconversion detection.

4. Conclusion

In conclusion, we have experimentally demonstrated a paradigm of TE/TM polarization-independent frequency upconversion by leveraging polarization coupling and SFG in the PPLNOI ridge waveguide. Taking advantage of the LNOI ridge waveguide, low voltage and enhanced conversion efficiency can be obtained. The TE/TM polarization-independent operation can be accessed at different wavelengths via temperature tuning. The demonstrated method may find ready applications in all-optical wavelength conversion and upconversion detection technologies.

Acknowledgement

This work was supported by the National Natural Science Foundation of China (Nos. 12074252, 12192252, 62005159, 62022058, 61705127, and 12104289), the National Key Research and Development Program of China (No. 2018YFA0306301), the Shanghai Municipal Science and Technology Major Project (No. 2019SHZDZX01-ZX06), the Shanghai Rising-Star Program (No. 20QA1405400), and the Yangyang Development Fund.

References

1. R. W. Boyd, *Nonlinear Optics*, 3rd ed. (Academic Press, 2008).
2. Y. Niu, X. Yan, J. Chen, Y. Ma, Y. Zhou, H. Chen, Y. Wu, and Z. Bai, "Research progress on periodically poled lithium niobate for nonlinear frequency conversion," Infrared Phys. Technol. **125**, 104243 (2022).
3. Y. Li, Z. Huang, W. Qiu, J. Dong, H. Guan, and H. Lu, "Recent progress of second harmonic generation based on thin film lithium niobate," Chin. Opt. Lett. **19**, 060012 (2021).
4. T. Wang, P. Chen, C. Xu, Y. Zhang, D. Wei, X. Hu, G. Zhao, M. Xiao, and S. Zhu, "Periodically poled $LiNbO_3$ crystals from 1D and 2D to 3D," Sci. China Technol. Sci. **63**, 1110 (2020).
5. Y. L. Lee, B. A. Yu, T. J. Eom, W. Shin, C. Jung, Y. C. Noh, J. Lee, D. K. Ko, and K. Oh, "All-optical AND and NAND gates based on cascaded second-order nonlinear processes in a Ti-diffused periodically poled $LiNbO_3$ waveguide," Opt. Express **14**, 2776 (2006).
6. H. Hu, R. Nouroozi, R. Ludwig, B. Huettl, C. Schmidt-Langhorst, H. Suche, W. Sohler, and C. Schubert, "Polarization-insensitive all-optical wavelength conversion of 320 Gb/s RZ-DQPSK signals using a Ti:PPLN waveguide," Appl. Phys. B **101**, 875 (2010).
7. Q. Guo, R. Sekine, L. Ledezma, R. Nehra, D. J. Dean, A. Roy, R. M. Gray, S. Jahani, and A. Marandi, "Femtojoule femtosecond all-optical switching in lithium niobate nanophotonics," Nat. Photonics **16**, 625 (2022).
8. M. Mrejen, Y. Erlich, A. Levanon, and H. Suchowski, "Multicolor time-resolved upconversion imaging by adiabatic sum frequency conversion," Laser Photonics Rev. **14**, 2000040 (2020).
9. J. S. Pelc, L. Ma, C. R. Phillips, Q. Zhang, C. Langrock, O. Slattery, X. Tang, and M. M. Fejer, "Long-wavelength-pumped upconversion single-photon detector at 1550 nm: performance and noise analysis," Opt. Express **19**, 21445 (2011).
10. K. Huang, J. Fang, M. Yan, E. Wu, and H. Zeng, "Long-wavelength-pumped upconversion single-photon detector at 1550 nm: performance and noise analysis," Nat. Commun. **13**, 1077 (2022).
11. S. Wang, N. Yao, W. Fang, and L. Tong, "Polarization-independent photon up-conversion with a single lithium niobate waveguide," Opt. Express **30**, 2817 (2022).
12. P. G. Kwiat, E. Waks, A. G. White, I. Appelbaum, and P. H. Eberhard, "Ultrabright source of polarization-entangled photons," Phys. Rev. A **60**, R773(R) (1999).
13. H.-J. Wu, B. Zhao, C. Rosales-Guzmán, W. Gao, B.-S. Shi, and Z.-H. Zhu, "Spatial-polarization-independent parametric up-conversion of vectorially structured light," Phys. Rev. Appl. **13**, 064041 (2020).
14. H. Liu, H. Li, Y. Zheng, and X. Chen, "Nonlinear frequency conversion and manipulation of vector beams," Opt. Lett. **43**, 5981 (2018).
15. R. Ikuta, T. Kobayashi, T. Kawakami, S. Miki, M. Yabuno, T. Yamashita, H. Terai, M. Koashi, T. Mukai, T. Yamamoto, and N. Imoto, "Polarization insensitive frequency conversion for an atom-photon entanglement distribution via a telecom network," Nat. Commun. **9**, 1997 (2018).
16. H. Takesue, E. Diamanti, C. Langrock, M. M. Fejer, and Y. Yamamoto, "1.5-μm single photon counting using polarization-independent up-conversion detector," Opt. Express **14**, 13067 (2006).
17. L.-Y. Liang, J.-S. Liang, Q. Yao, M.-Y. Zheng, X.-P. Xie, H. Liu, Q. Zhang, and J.-W. Pan, "Compact all-fiber polarization-independent up-conversion single-photon detector," Opt. Commun. **441**, 185 (2019).
18. D. Zhu, L. Shao, M. Yu, R. Cheng, B. Desiatov, C. J. Xin, Y. Hu, J. Holzgrafe, S. Ghosh, A. Shams-Ansari, E. Puma, N. Sinclair, C. Reimer, M. Zhang, and M. Lončar, "Integrated photonics on thin-film lithium niobate," Adv. Opt. Photon. **13**, 242 (2021).
19. J. Lin, F. Bo, Y. Cheng, and J. Xu, "Advances in on-chip photonic devices based on lithium niobate on insulator," Photonics Res. **8**, 1910 (2020).
20. G. Chen, N. Li, J. D. Ng, H.-L. Lin, Y. Zhou, Y. H. Fu, L. Y. T. Lee, Y. Yu, A.-Q. Liu, and A. J. Danner, "Advances in lithium niobate photonics: development status and perspectives," Adv. Photonics **4**, 034003 (2022).
21. A. Caspar, M. Roussey, M. Häyrinen, J. Laukkanen, A. Pérignon, F. Behague, V. Calero, G. Ulliac, M.-P. Bernal, M. Kuittinen, and N. Courjal, "High-aspect-ratio $LiNbO_3$ ridge waveguide with vertical buffer layer and enhanced electro-optical efficiency," J. Lightwave Technol. **36**, 2702 (2018).
22. C. Wang, M. Zhang, X. Chen, M. Bertrand, A. Shams-Ansari, S. Chandrasekhar, P. Winzer, and M. Lončar, "Integrated lithium niobate electro-optic modulators operating at CMOS-compatible voltages," Nature **562**, 101 (2018).
23. M. He, M. Xu, Y. Ren, J. Jian, Z. Ruan, Y. Xu, S. Gao, S. Sun, X. Wen, L. Zhou, L. Liu, C. Guo, H. Chen, S. Yu, L. Liu, and X. Cai, "High-performance hybrid silicon and lithium niobate Mach–Zehnder modulators for 100 Gbit s^{-1} and beyond," Nat. Photonics **13**, 359 (2019).
24. T. Ding, Y. Zheng, and X. Chen, "On-chip Solc-type polarization control and wavelength filtering utilizing periodically poled lithium niobate on insulator (PPLNOI) ridge waveguide," J. Lightwave Technol. **37**, 1296 (2019).
25. F. Thiele, F. vom Bruch, V. Quiring, R. Ricken, H. Herrmann, C. Eigner, C. Silberhorn, and T. J. Bartley, "Cryogenic electro-optic polarisation conversion in titanium in-diffused lithium niobate waveguides," Opt. Express **28**, 28961 (2020).
26. Z. Lin, Y. Lin, H. Li, M. Xu, M. He, W. Ke, H. Tan, Y. Han, Z. Li, D. Wang, X. S. Yao, S. Fu, S. Yu, and X. Cai, "High-performance polarization management devices based on thin-film lithium niobate," Light Sci. Appl. **11**, 93 (2022).
27. T. Ding, Y. Zheng, and X. Chen, "Integration of cascaded electro-optic and nonlinear processes on a lithium niobate on insulator chip," Opt. Lett. **44**, 1524 (2019).
28. D. Wang, T. Ding, Y. Zheng, and X. Chen, "Cascaded sum-frequency generation and electro-optic polarization coupling in the PPLNOI ridge waveguide," Opt. Express **27**, 15283 (2019).
29. C.-Y. Cho, J.-Y. Lai, C.-S. Hsu, Y.-T. Huang, J.-H. Jang, and M.-H. Chou, "Power scaling of continuous-wave second harmonic generation in a MgO:PPLN ridge waveguide and the application to a compact wavelength conversion module," Opt. Lett. **46**, 2852 (2021).